RSC Advances

PAPER

View Article Online
View Journal | View Issue

Cite this: *RSC Adv.*, 2022, **12**, 4276

Single-pot tandem oxidative/C–H modification amidation process using ultrasmall Pd_{NP}-encapsulated porous organosilica nanotubes†

Behnam Gholipour, [a] Afsaneh Zonouzi,*[a] Sadegh Rostamnia *[b] and Xiao Liu *[c]

Received 27th November 2021
Accepted 16th January 2022

DOI: 10.1039/d1ra08682k

rsc.li/rsc-advances

Herein, we studied a single-pot method with a dual catalysis process towards the conversion of primary aromatic alcohols to amides using ultrasmall Pd_{NPs} of controlled uniform size (1.8 nm) inside hybrid mesoporous organosilica nanotubes (MO-NTs). The catalyst exhibited excellent performance in water under mild conditions and showed high stability. The catalytic activity towards the tandem oxidation of alcohols in the presence of amine salts and H_2O_2 to their corresponding amides without producing byproducts was evaluated, and high yields were obtained for all products. The structure of the organosilica nanotubes containing palladium nanoparticles was investigated using various characterization techniques such as XRD, TEM, BET, solid-state ^{29}Si NMR and solid-state ^{13}C CP MAS NMR. Catalyst recycling tests showed that the catalytic power of PdNPs@B-SNTs was preserved after 8 cycles and a slight decrease in catalyst activity was observed.

1. Introduction

In a multitude of chemical structures, amide functional groups are important organic units. Moreover, due to the desirable properties of amides, such as high polarity, stability and conformational diversity, they have become one of the most beloved and reliable application groups in all branches of organic chemistry.[1] For the formation of amide bonds, due to the applicability of this group in biological molecules, chemicals and pharmaceuticals, atom-efficient and green methods are a long-term consideration and a challenge in both research and industrial chemistry.[2] Meanwhile, for diverse biologically active compounds and pharmaceuticals, primary and secondary amides are synthetically vital key intermediates as well as impressive progenitors.[3] Among the methods proposed for the synthesis of amides, the use of alcohols has become one of the best alternatives. Indeed, alcohols can be converted to amides through a tandem oxidation process under oxidative conditions *in situ via* carboxylic acids or aldehydes[4–19] (Scheme 1).

In line with sustainable development and green chemistry, the utilization of heterogeneous catalysts *versus* conventional homogeneous catalysts has captured increasing attention.[20] Among the heterogeneous catalysts, solid-based catalysts have many advantages such as lower corrosiveness, fewer disposal rates, and a higher selectivity to target products, as well as the simple separation of catalysts as an environmentally benign and economical route for the synthesis of chemicals.[21] In this regard, the performance of heterogeneous catalysts can be amended by engineering the porosity of a solid catalyst to create a larger specific surface area, in addition to other parameters.[22] In recent years, ordered mesoporous silica (OMS) has attracted research consideration in the field of catalysis because of its long-range order, high surface area, uniform silanol surface, ease of being functionalized, tunable hydrophobicity/hydrophilicity, periodically ordered pores (2–50 nm) and nanometer-thick walls.[23] Accordingly, the immobilization of metal nanoparticles in solid supports such as PMO is an attractive strategy, which in addition to increasing lipophilicity can improve their recovery and diminish their tendency to agglomerate and leach.[24] For this reason, many attempts have been reported that use PMOs for organic transformations, including $Pd_{(nano)}$/MNP@IL-SiO_2,[25] Fe_3O_4@SiO_2@PMO,[26] Pd-MPMO,[27] Sc$(OTf)_2$-SO_3Ph-PMO,[28] Cu@PMO NCs,[29] Porph@PMO and Pic@PMO.[30] Despite the remarkable success of active and efficient heterogeneous catalysts, the design and development of sustainable and green catalysts continues to be an important and imperative challenge.

Our groups succeeded in engineering periodic mesoporous organosilicas (PMOs)[31–37] and 1D organosilica nanotube linkages with organic ethane and phenylene groups.[38] To further develop the application of organosilica nanotubes, we reported the enhanced durability of Ir-BPy-NT for water oxidation,[39] PCN-

[a]*School of Chemistry, College of Science, University of Tehran, P.O. Box 14155-6455, Tehran, Iran. E-mail: b.gholipour@ut.ac.ir; zonouziafsaneh@ut.ac.ir*

[b]*Organic and Nano Group (ONG), Department of Chemistry, Iran University of Science and Technology (IUST), PO Box 16846-13114, Tehran, Iran. E-mail: rostamnia@iust.ac.ir; srostamnia@gmail.com*

[c]*Key Laboratory of Pesticide & Chemical Biology of the Ministry of Education, College of Chemistry, Central China Normal University, Wuhan 430079, P. R. China. E-mail: liuxiao71@tju.edu.cn*

† Electronic supplementary information (ESI) available. See DOI: 10.1039/d1ra08682k

SNT and PCN-BSNT as efficient photocatalysts for H_2 generation[40] and metal-free amino-incorporated organosilica nanotubes for the cycloaddition of CO_2 to epoxides.[41] In this work, in order to achieve an efficient and practical protocol, we developed the use of stabilized Pd nanoparticles in the inner channels of organosilica nanotubes assembled with 1,4-bis(triethoxysilyl)benzene and P123 precursors as active and reusable hybrid catalysts for the synthesis of primary and secondary amides in single-pot and mild conditions (Scheme 1).

2. Experimental

2.1. Chemicals and reagents

Triblock copolymer EO20PO70EO20 (Pluronic P123), 1,4-bis(-triethoxysilyl)benzene (BTEB), tetraethoxysilane (99%, TEOS), and other reagents were purchased from Sigma-Aldrich (Shanghai Chemical Reagent., Inc. of Chinese Medicine Group). All materials were of analytical grade and used without any further purification.

2.2. Characterization

Powder X-ray diffraction (PXRD) patterns were recorded on a Rigaku RINT D/Max-2500 powder diffraction system using Cu Kα radiation of 0.15406 nm wavelength over a 2θ range of 15–90° at a scan speed of 5° min^{-1} at room temperature. Nitrogen and water sorption experiments were performed at 77 K and 293 K, respectively, on a Micromeritics ASAP 2020 system. Prior to the measurement, the samples were out-gassed at 120 °C for at least 6 h. The Brunauer–Emmett–Teller (BET) specific surface areas were calculated using the adsorption data at a relative pressure range of $P/P_0 = 0.05$–0.25. Pore size distributions were calculated from the adsorption branch using the Barrett–Joyner–Halenda (BJH) method. The total pore volumes were estimated from the amount adsorbed at a relative pressure (P/P_0) of 0.99. Transmission electron microscopy (TEM) was performed using an FEI Tecnai G2 Spirit at an acceleration voltage of 120 kV. ^{13}C (100.5 MHz) cross-polarization magic angle spinning (CP-MAS) and ^{29}Si (79.4 MHz) MAS solid-state NMR experiments were conducted on a Varian Infinity-Plus 400 spectrometer equipped with a magic-angle spin probe in a 4 mm ZrO_2 rotor. ^{13}C and ^{29}Si signals were referenced to tetramethylsilane. The experimental parameters were an 8 kHz spin rate, 3 s pulse delay, 4 min contact time, and 1500–3000 scans for the ^{13}C CP-MAS NMR experiments, and a 4 kHz spin rate, 180 s pulse delay, 10 min contact time, and 116 scans for the ^{29}Si MAS NMR experiments.

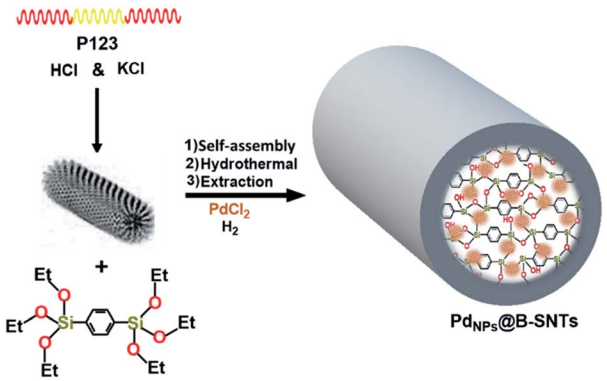

Fig. 1 Schematic illustration of the procurement of Pd_{NPs}@B-SNTs.

2.3. Synthesis of benzene-silica nanotubes (B-SNTs)

According to a previous report on the synthesis of benzene-silica nanotubes,[38] 0.55 g P123 and 3.49 g KCl were dissolved in

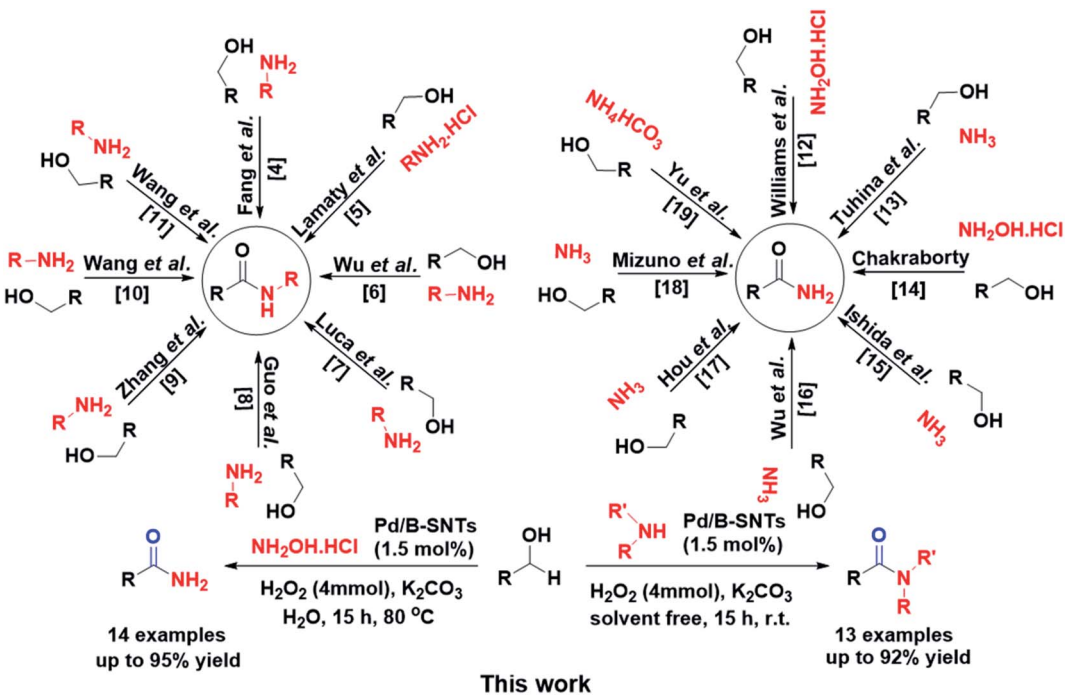

Scheme 1 General route for tandem oxidative amidation.

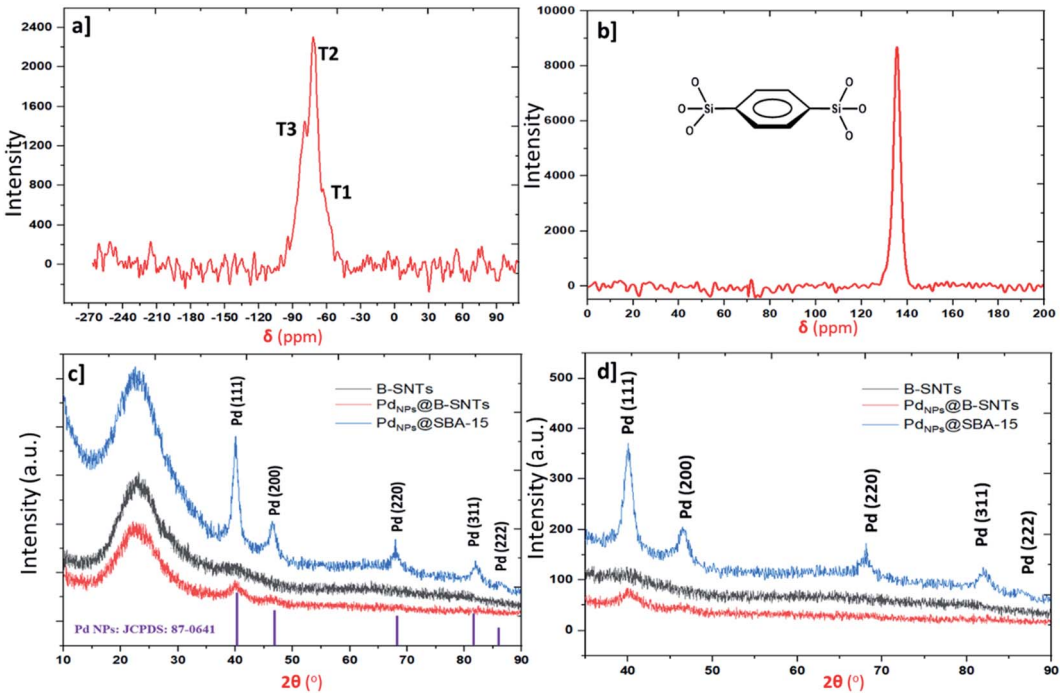

Fig. 2 (a) ^{29}Si NMR spectrum of the B-SNTs. (b) ^{13}C CP MAS NMR spectra of the B-SNTs. (c) and (d) XRD patterns of Pd$_{NPs}$@B-SNTs and Pd$_{NPs}$@SBA-15.

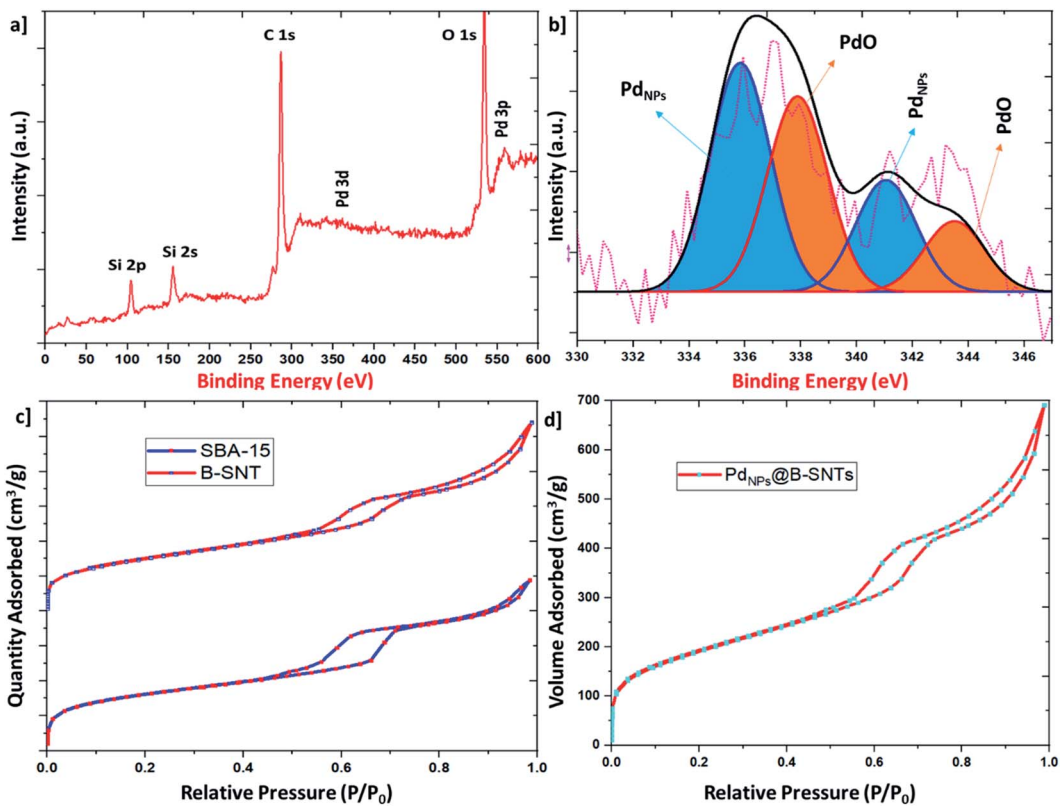

Fig. 3 (a) and (b) XPS spectra of Pd$_{NPs}$@B-SNTs. (c) and (d) Nitrogen adsorption–desorption isotherms of the B-SNTs, SBA-15 and PdNPs/B-SNTs.

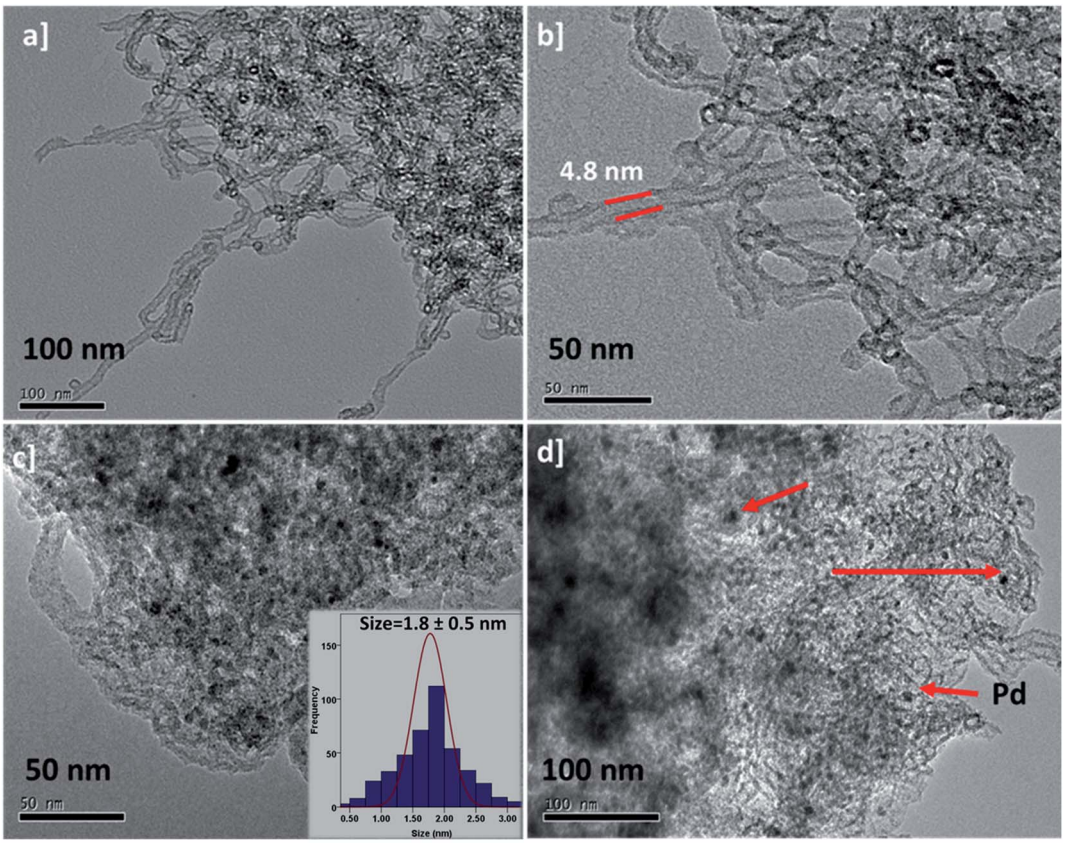

Fig. 4 (a) and (b) TEM images of the B-SNTs and (c) and (d) PdNPs@B-SNTs, and the average diameter histogram of the Pd_{NPs} for Pd_{NPs}@B-SNTs.

Table 1 Specific surface area (S_{BET}), pore diameter and total pore volume

Sample	BET surface area ($cm^3\ g^{-1}$)	Pore diameter (nm)	Total pore volume ($cm^3\ g^{-1}$)
B-SNT	701	5.5	0.79
Pd_{NPs}-B-SNT	690	6.1	1.07
SBA-15	835.4	6.8	1.12

180 mL 2 M HCl at 38 °C. After complete copolymer dissolution, 3.50 mmol 1,4-bis(triethoxysilyl)benzene (BTEB) was added under vigorous shaking for 6 min, and the resulting mixture was kept for 24 h at the same temperature. Subsequently, the mixture was treated at 100 °C under static conditions for 24 h. The solid product was recovered by filtration and air-dried at ambient temperature overnight. Finally, for the extracted surfactant, 1.0 g of the as-synthesized solid in 200 mL of ethanol containing 1.5 g concentrated aqueous HCl solution was refluxed for 24 h.

2.4. Encapsulation of Pd particles in the benzene-silica nanotubes (Pd_{NPs}@B-SNTs)

For the synthesis of Pd_{NPs}@B-SNTs, B-SNTs (0.3 g) were added to 10 mL ethanol solution containing $PdCl_2$ (0.026 g). After 1 h of ultrasonic treatment, the solution was stirred at room temperature for 12 h. Finally, the obtained solids were reduced at 150 °C in H_2 for 5 h.

2.5. Synthesis of SBA-15 and the encapsulation of Pd particles in the pores

Synthesis of SBA-15 using an aqueous solution of the Pluronic copolymer P123 (E21P67E21), 2 M HCl and tetraethyl orthosilicate (TEOS) was executed step-by-step according to our previous method.[42–54] Loading of Pd_{NPs} in SBA-15 pore channels was performed according to the abovementioned method.

2.6. General procedure for the synthesis of primary and secondary amides

To synthesize primary and secondary amides, mixtures of preliminary substrates (amine salts and benzyl alcohol) in separate dry vials were subjected to intense stirring under obtained optimal conditions (Scheme 1). After the specified time, the reaction mixture was diluted in CH_2Cl_2/H_2O solution (1 : 1). After rinsing the organic phase with H_2O several times (3 × 10 mL), the CH_2Cl_2 solvent was separated with a rotary. Finally, purification was performed *via* chromatography on silica gel (hexanes/EtOAc).

3. Results and discussion

Fig. 1 summarizes the preparation of organosilica nanotubes to support palladium nanoparticles for the sustainable and green synthesis of primary and secondary amides. Benzene-bridged organosilica nanotubes (B-SNTs) were constructed with the incorporation of covalently bonded organic–inorganic 1,4-

Table 2 Optimization of reaction conditions[a]

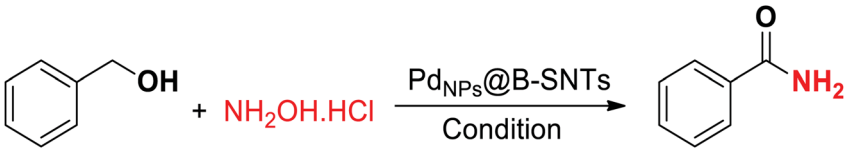

Entry	Catalyst	Oxidant (mmol)	Solvent	Base	Pd (mol%)	T (°C)	Time (h)	Yield[b] (%)
1	Pd_{NPs}@B-SNTs	H_2O_2 (1)	H_2O	K_2CO_3	1	80	24	60
2	Pd_{NPs}@B-SNTs	H_2O_2 (2)	H_2O	K_2CO_3	1	80	24	75
3	Pd_{NPs}@B-SNTs	H_2O_2 (3)	H_2O	K_2CO_3	1	80	20	85
4	**Pd_{NPs}@B-SNTs**	**H_2O_2 (4)**	**H_2O**	**K_2CO_3**	**1**	**80**	**20**	**95**
5	Pd_{NPs}@SBA-15	H_2O_2 (4)	H_2O	K_2CO_3	1	80	20	80
6	Pd_{NPs}@B-SNTs	H_2O_2 (4)	H_2O	K_2CO_3	1	100	20	95
7	Pd_{NPs}@B-SNTs	H_2O_2 (4)	H_2O	K_2CO_3	0.5	80	24	60
8	Pd_{NPs}@B-SNTs	H_2O_2 (4)	H_2O	K_2CO_3	1.5	80	20	95
9	Pd_{NPs}@B-SNTs	H_2O_2 (4)	H_2O	K_2CO_3	1	60	24	70
10	Pd_{NPs}@B-SNTs	H_2O_2 (4)	H_2O	K_2CO_3	1	r.t.	24	40
11	Pd_{NPs}@B-SNTs	MnO_2 (4)	H_2O	K_2CO_3	1	80	20	25
12	Pd_{NPs}@B-SNTs	TBHP (4)	H_2O	K_2CO_3	1	80	20	80
13	Pd_{NPs}@B-SNTs	SeO_2 (4)	H_2O	K_2CO_3	1	80	20	30
14	Pd_{NPs}@B-SNTs	H_2O_2 (4)	H_2O	NaOAc	1	80	20	35
15	Pd_{NPs}@B-SNTs	H_2O_2 (4)	H_2O	$NaHCO_3$	1	80	20	25
16	Pd_{NPs}@B-SNTs	H_2O_2 (4)	H_2O	Na_2CO_3	1	80	20	92
17	Pd_{NPs}@B-SNTs	H_2O_2 (4)	H_2O	Cs_2O_3	1	80	20	95
18	Pd_{NPs}@B-SNTs	H_2O_2 (4)	H_2O	NEt_3	1	80	20	40
19	Pd_{NPs}@B-SNTs	H_2O_2 (4)	H_2O	Py	1	80	20	30
20	Pd_{NPs}@B-SNTs	H_2O_2 (4)	H_2O	—	1	80	20	—
21	—	H_2O_2 (4)	H_2O	K_2CO_3	1	80	20	—
22	Pd_{NPs}@B-SNTs	H_2O_2 (4)	Ethanol	K_2CO_3	1	80	20	75
23	Pd_{NPs}@B-SNTs	H_2O_2 (4)	Dioxane	K_2CO_3	1	80	20	50
24	Pd_{NPs}@B-SNTs	H_2O_2 (4)	DMSO	K_2CO_3	1	80	20	55
25	Pd_{NPs}@B-SNTs	H_2O_2 (4)	Toluene	K_2CO_3	1	80	20	20
26	Pd_{NPs}@B-SNTs	H_2O_2 (4)	DMF	K_2CO_3	1	80	20	65

[a] Reaction conditions: benzaldehyde (1 mmol), $NH_2OH{\cdot}HCl$ (1 mmol), base (1.5 mmol), H_2O_2 (4 mmol) in 3 mL of solvent. [b] Isolated yield.

bis(triethoxysilyl)benzene (BTEB) ligands in the presence of P123 under acidic conditions, and the template was extracted using EtOH. Then, the as-synthesized B-SNTs were utilized for the encapsulation of palladium nanoparticles inside the pore channels.

Solid-state ^{29}Si NMR spectrum of the B-SNTs indicates the existence of T^n sites (Fig. 2a). The signals at −60.7, −70.2 and −80.3 ppm in the spectrum of the B-SNTs represent the silicone species T^1 [$SiC(OH)_2(OSi)$], T^2 [$SiC(OH)(OSi)_2$], and T^3 [$SiC(OSi)_3$], respectively, which confirm that the full framework joined the organosilica nanotubes. The lack of SiO_4 species, such as Q^3 [$Si(OH)(OSi)_3$] and Q^4 [$Si(OSi)_4$], in the range of −90 to −120 ppm confirms that no carbon–silicon bond fracture occurred during the synthesis of the organosilica nanotubes.[31] The chemical shift at 133.4 ppm is related to the signal of the benzene ring. The signals at 71.5, 55.6 and 18.8 ppm correspond to the remaining surfactants and ethoxy carbon groups formed during the surfactant extraction process (Fig. 2b).[31] Wide-angle XRD analysis was used to confirm the structure and crystallinity of the as-synthesized Pd_{NPs} inside the B-SNTs and SBA-15. The scatter pattern for the Pd nanoparticles with five specific reflections at 40.06 (1 1 1), 47.02 (2 0 0), 68.03 (2 2 0), 81.68 (3 1 1) and 86.32 (2 2 2) shows that these characteristic reflections are related to the cubic (fcc) structure of the Pd_{NPs} (JCPDS: 87-0641, space group: *Fm3m* (225)) (Fig. 2c and d).[38]

The surface oxidation and chemical modes of the Pd_{NPs}@B-SNT catalysts were analyzed by XPS spectroscopy. Fig. 3a exhibits the XPS spectra of Pd_{NPs}@B-SNTs. Several distinct peaks were observed in the XPS survey spectra at ∼105, ∼157, ∼290, ∼335–345, ∼537 and ∼560 eV, corresponding to Si 2p, Si 2s, C 1s, Pd 3d, O 1s and Pd 3p, respectively. The Pd_{NPs}@B-SNT spectrum revealed in Fig. 3b shows the presence of two chemical states of Pd. The binding energy range of 335–341 eV is correlated to Pd $3d_{5/2}$ and Pd $3d_{3/2}$ of metallic Pd, while the component at 338–344 eV is related to PdO owing to the partial oxidation of the Pd_{NPs}.[55,56] The surface area, pore volume and diameter of the B-SNTs and Pd_{NPs}@B-SNTs are calculated based on the Brunauer–Emmett–Teller (BET) equation (Table 1).

Nitrogen adsorption and desorption isotherms of the B-SNTs, SBA-15 and Pd_{NPs}@B-SNTs are shown in Fig. 3c and d. The hysteresis ring at a pressure of P/P_0 = 0.5–0.7, which is consistent with the mesoporous materials, indicates the maintenance of the structure of the B-SNTs and Pd_{NPs}@B-SNTs after the loading of Pd nanoparticles. The decrease in the BET

Table 3 Tandem oxidation of various primary aromatic alcohols to primary amides using Pd_{NPs}@B-SNTs[a]

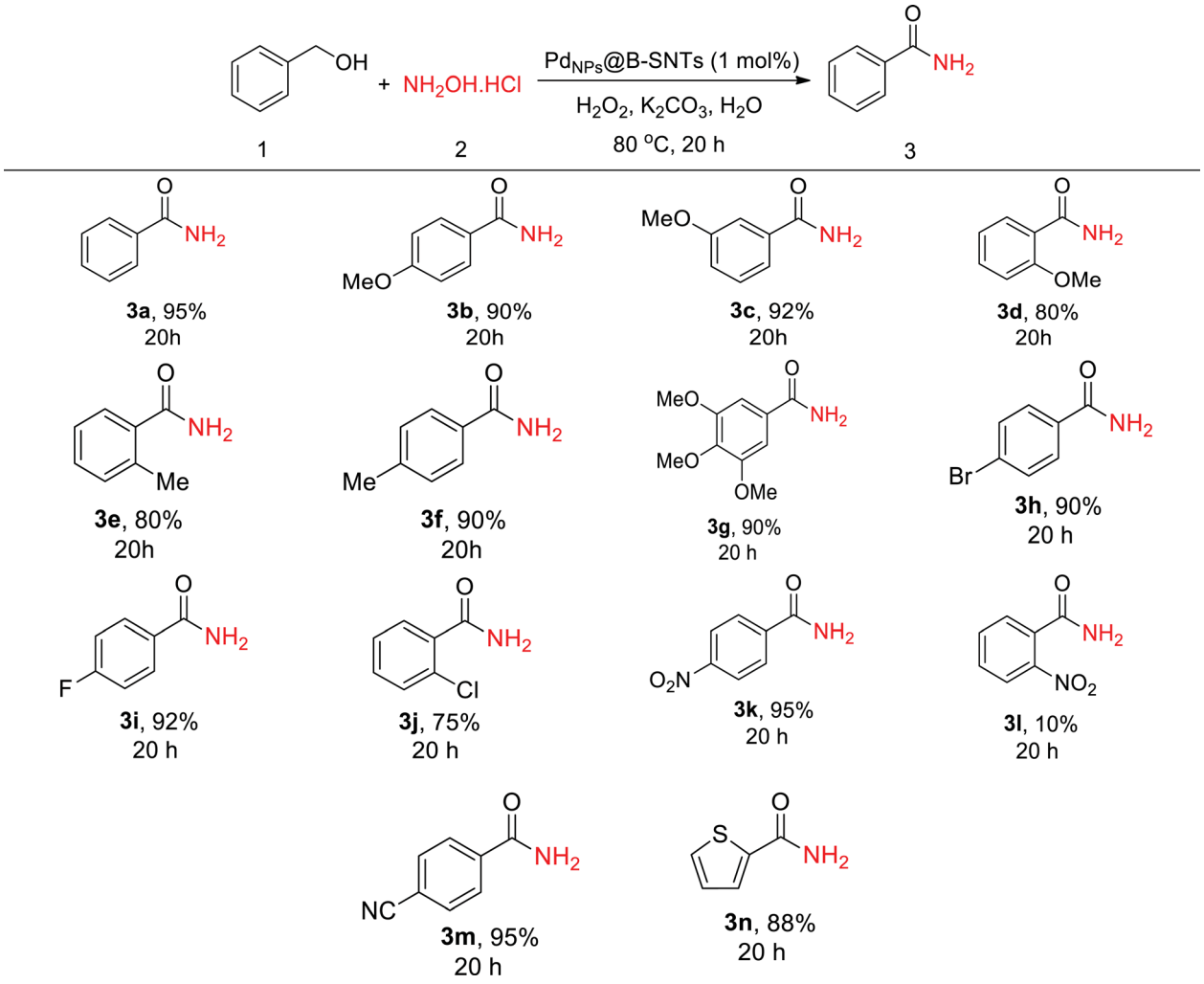

[a] Reaction condition: alcohol (1 mmol), $NH_2OH{\cdot}HCl$ (1 mmol), K_2CO_3 (1.5 mmol), H_2O_2 (4 mmol) in 3 mL H_2O at 80 °C.

surface area of Pd_{NPs}@B-SNTs is attributed to the presence of Pd nanoparticles loaded inside the B-SNT channels, leading to the partial obstruction of the channels. A small difference in the surface areas of the B-SNTs and SBA-15 might be due to the presence of 1,4-bis(triethoxysilyl)benzene (BTEB) ligands in the B-SNTs.

Fig. 4a–d illustrates the TEM images of the B-SNTs before and after the encapsulation of palladium nanoparticles. The TEM images clearly demonstrate that the Pd nanoparticles are evenly distributed in the inner channel of the B-SNTs. Based on the TEM images, the size of the Pd_{NPs} in the B-SNTs is 1.8 nm. According to the results of TEM, the occurrence of much smaller Pd nanoparticles in the B-SNTs might be due to the stabilizing effect of the benzene ring in the B-SNT network.

In line with the development of sustainable protocols and inspired by our previous work on the catalytic application of solid-based catalysts and porous materials (PMO, SBA-15, and MOF) in organic reaction transformations,[31,34,52,53,55–65] especially the synthesis of amides,[66–70] herein, we describe a one-pot tandem oxidative amidation reaction using Pd_{NPs}@B-SNTs as an active catalyst and H_2O_2 as a green oxidant for the synthesis of primary, secondary, and tertiary amides. The catalytic activity domain of Pd_{NPs}@B-SNTs for the synthesis of amides using various structural compounds (primary aromatic and aliphatic alcohols, amine salts, and $NH_2OH{\cdot}HCl$) through oxidative amidation was evaluated. The results are further elaborated and summarized in Table 2, and the reaction conditions such as different bases, oxidants, solvent and the amount of catalyst are explored. Assuming that the addition of water as a green solvent might increase product yields, it was used as the preliminary solvent. Initially, benzyl alcohol, hydroxylammonium chloride and K_2CO_3 (1 : 1 : 1.5 ratio) were selected for a model reaction in the presence of H_2O_2 (30%). First, the effects of H_2O_2 and Pd_{NP} amount using H_2O as a solvent at 80 °C for the formation of amide were investigated. Comparison of the different values of H_2O_2 and Pd_{NPs} showed that the use of 4 mmol H_2O_2 and

Table 4 Investigation of Pd_{NPs}@B-SNTs in the presence of various types of oxidants[a]

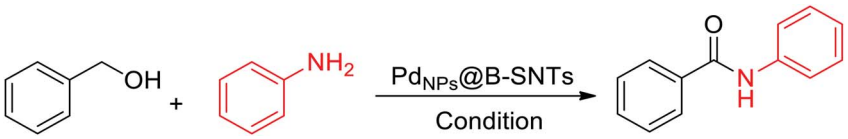

Entry	Catalyst	Pd (mol%)	Base	[O]	T (°C)	Time (h)	Yield[b] (%)
1	Pd_{NPs}@B-SNTs	0.5	K_2CO_3	H_2O_2 (2 mmol)	25	20	70
2	Pd_{NPs}@B-SNTs	1	K_2CO_3	H_2O_2 (2 mmol)	25	20	78
3	Pd_{NPs}@B-SNTs	1	K_2CO_3	H_2O_2 (4 mmol)	25	20	80
4	**Pd_{NPs}@B-SNTs**	**1.5**	**K_2CO_3**	**H_2O_2 (4 mmol)**	**25**	**15**	**92**
5	Pd_{NPs} @SBA-15	1.5	K_2CO_3	H_2O_2 (4 mmol)	25	15	78
6	Pd_{NPs}@B-SNTs	1.5	K_2CO_3	DDQ (4 mmol)	25	15	25
7	Pd_{NPs}@B-SNTs	1.5	K_2CO_3	NaClO (4 mmol)	25	15	20
8	Pd_{NPs}@B-SNTs	1.5	K_2CO_3	MnO_2 (4 mmol)	25	15	35
9	Pd_{NPs}@B-SNTs	1.5	K_2CO_3	SeO_2 (4 mmol)	25	15	30
10	Pd_{NPs}@B-SNTs	1.5	K_2CO_3	TBHP (4 mmol)	25	15	70
11	Pd_{NPs}@B-SNTs	1.5	Na_2CO_3	H_2O_2 (4 mmol)	25	15	85
12	Pd_{NPs}@B-SNTs	1.5	NaOAc	H_2O_2 (4 mmol)	25	15	40
13	Pd_{NPs}@B-SNTs	1.5	$NaHCO_3$	H_2O_2 (4 mmol)	25	15	35
14	Pd_{NPs}@B-SNTs	1.5	Cs_2CO_3	H_2O_2 (4 mmol)	25	15	88
15	Pd_{NPs}@B-SNTs	1.5	K_3PO_4	H_2O_2 (4 mmol)	25	15	25
16	Pd_{NPs}@B-SNTs	1.5	NEt_3	H_2O_2 (4 mmol)	25	15	30
17	Pd_{NPs}@B-SNTs	1.5	Py	H_2O_2 (4 mmol)	25	15	25
18	Pd_{NPs}@B-SNTs	1.5	—	H_2O_2 (4 mmol)	25	15	—
19	—	1.5	K_2CO_3	H_2O_2 (4 mmol)	25	15	—

[a] Reaction conditions: benzyl alcohol (1 mmol), aniline (1.2 mmol), base (1.5 mmol), oxidant (2–4 mmol) and Pd_{NPs}@B-SNTs (variant mol% of Pd) at room temperature in specific time. [b] Isolated yield.

1 mol% of Pd_{NPs} affords an excellent yield (Table 2, entries 1–10). On the other hand, the other oxidants did not show the desired yield compared to H_2O_2, except for TBHP (70% aqueous solution), which yielded 80% (Table 2, entries 11–13). In the different base study for the oxidative amidation of benzyl alcohol and hydroxyl ammonium chloride, the results of Cs_2CO_3 (95%) and K_2CO_3 (95%) were close, so K_2CO_3 was chosen as the appropriate base owing to its price and availability. No product was observed in the absence of a base. The results are summarized for other bases in Table 2 (entries 14–20). Furthermore, in the absence of a catalyst, no products were observed (Table 2, entry 21). A number of solvents including ethanol, dioxane, MeOH, toluene and DMSO were scrutinized in order to achieve further optimum conditions (Table 2). The catalyst performance was moderate in ethanol, dioxane, DMF, toluene and DMSO (yields of 20–75%), while amide yield was 95% in H_2O (Table 2, entries 22–26). As a result, H_2O was selected as the suitable solvent. The optimal conditions for Pd_{NPs}@B-SNTs were also evaluated for PdNPs@SBA-15 and a yield of 80% was obtained. The difference in the yield of the two studied catalysts could be related to the presence of aromatic phenyl groups in the body of the B-SNT channels, which increases the lipophilicity and thus leads to the effective mass transfer of organic lipophilic molecules to the inner surface of the channels to interact with the catalytic center.[23,71,72]

Taking into account the results obtained in Table 2, we examined the scope of the Pd-catalyzed tandem oxidative process for the synthesis of primary amides from primary aromatic alcohols and hydroxyl ammonium chloride under the optimized reaction conditions. Further screening of the electronic effect on the conversion of other alcohol derivatives into amides revealed that both electron-rich and electron-poor benzyl alcohols were successfully converted to their corresponding amides with high yield (Table 3). The results indicate that primary aromatic alcohols, particularly alcohols with electron withdrawing groups, are more active in the amidation reaction. A similar result was obtained with aromatic alcohols for heteroaromatic thiophene-2-carbaldehyde (Table 3).

In another method, the Pd_{NPs}@B-SNT catalyst was explored in one-pot tandem oxidative amidation reactions in the presence of H_2O_2 (30%) in solvent-free conditions. The catalytic activity of Pd_{NPs}@B-SNTs towards amide synthesis *via* the oxidative amidation of primary aromatic and aliphatic alcohols using aniline in the presence of H_2O_2 was evaluated as follows: Pd_{NPs}@B-SNTs (0.5 mol%), benzyl alcohol (1 mmol), aniline (1.2 mmol), H_2O_2 (2 mmol) and K_2CO_3 (1.5 mmol) were placed in a Teflon vessel with magnetic stirring at room temperature. Under these conditions, a conversion of 70% was obtained. By increasing the amount of Pd_{NPs} to 1.5 mol% and H_2O_2 to 4 mmol, the yield of conversion increased to 92% and the reaction time diminished to 12 h (Table 4, entries 1–5).

Table 5 Synthesis of amides with various types of alcohols and amines through oxidative amidation[a]

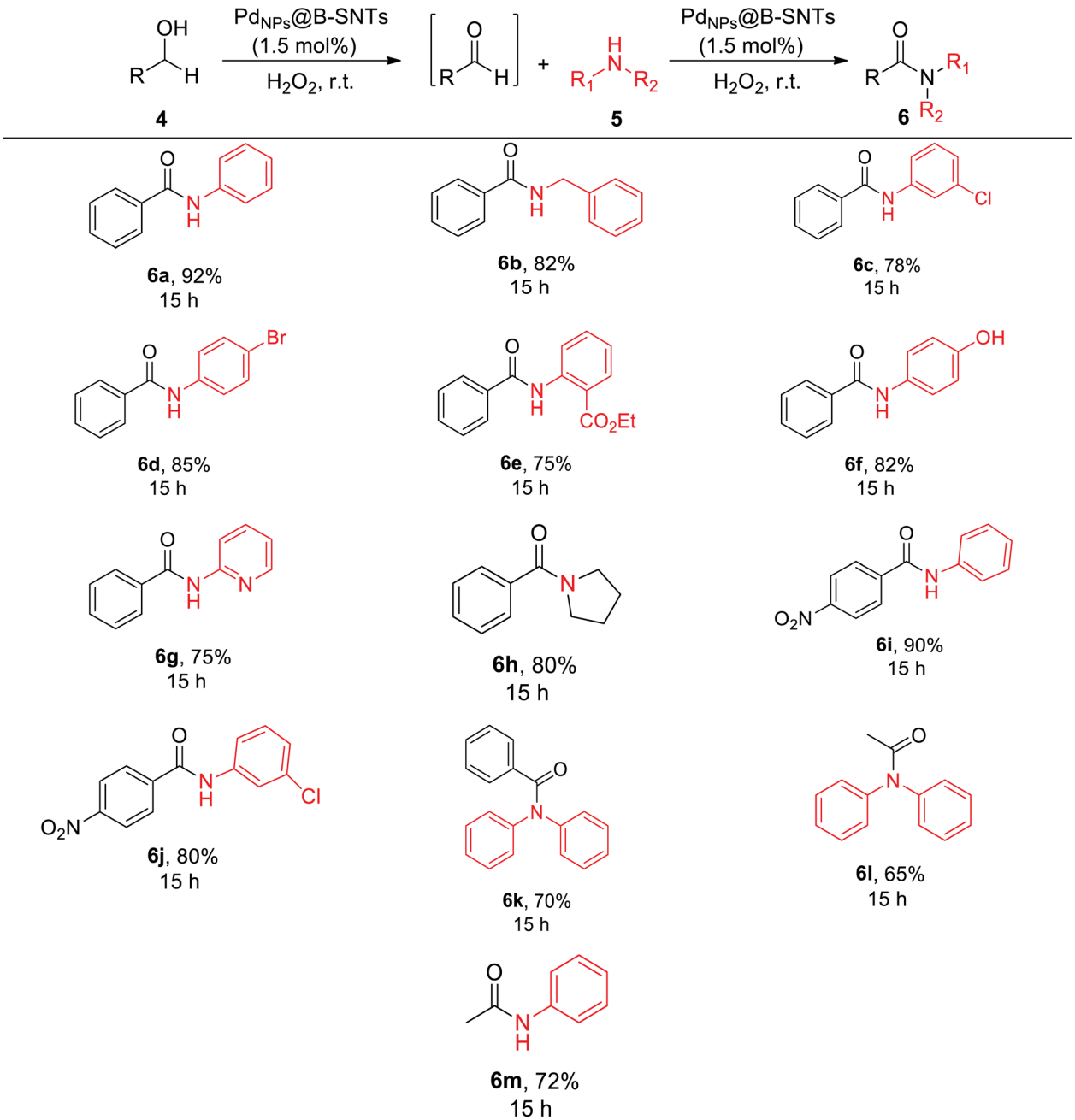

[a] Reaction conditions: benzyl alcohol (1 mmol), amine (1.2 mmol), base (1.5 mmol), H_2O_2 (4 mmol) and Pd$_{NPs}$@B-SNTs (1.5 mol% of Pd).

Examination of various oxidants such as SeO_2, MnO_2, DDQ, NaClO and TBHP in comparison with H_2O_2 shows that H_2O_2 leads to the rapid conversion of benzyl alcohol to the desired amide in the presence of aniline. The results of the various oxidants are summarized in Table 4 (entries 6–10). As shown in Table 4, the study of different bases shows that the conversion percentage is higher when K_2CO_3 is used compared to other bases (Table 4, entries 11–17). No product was observed in the absence of base or catalyst (Table 4, entries 18–19). In the case of Pd$_{NPs}$@SBA-15 *versus* Pd$_{NPs}$@B-SNTs, 78% yield was achieved, which according to the above explanation on primary amide synthesis is due to the existence of aromatic phenyl groups (Table 4, entry 5).

After achieving optimal conditions, further screening of the tandem oxidative reaction with different primary aromatic and aliphatic alcohols and various amines was performed to find the general mechanism and domain of the reaction. For all alcohol and amine derivatives with various substituents (Cl, Br, NO_2,

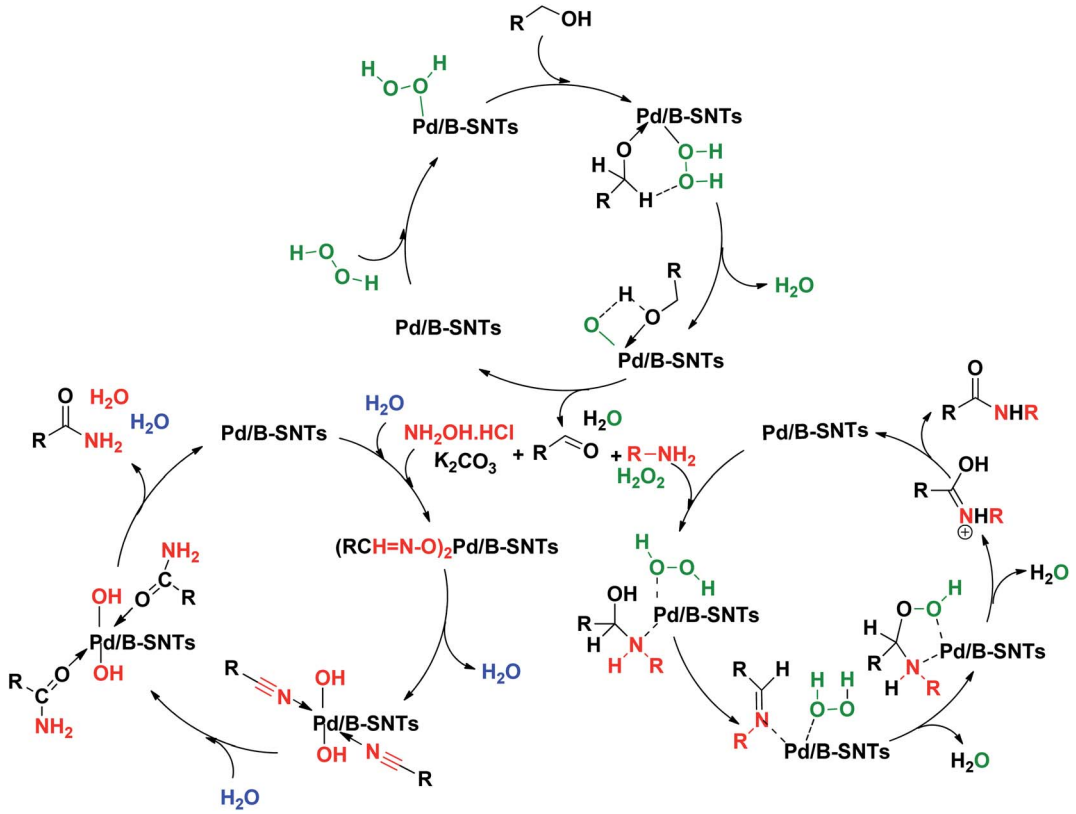

Scheme 2 General mechanism of tandem oxidative amidation.

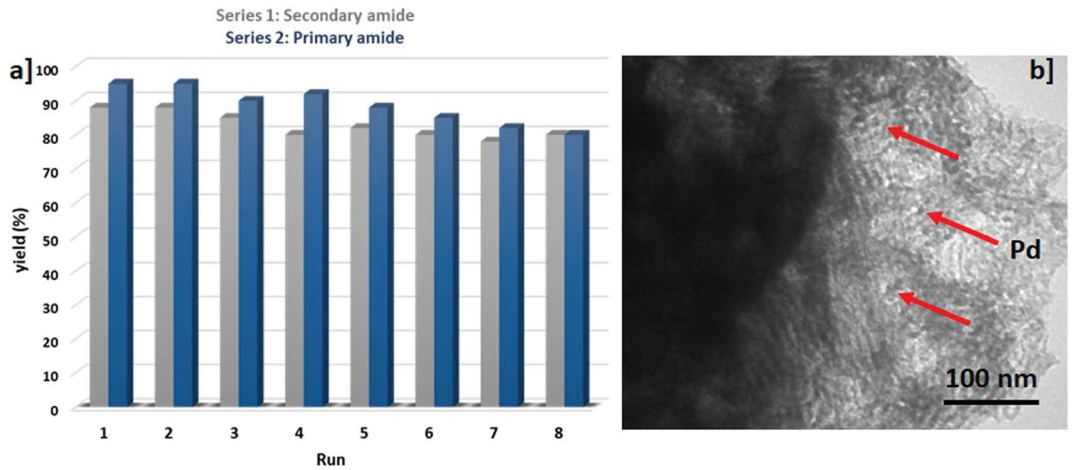

Fig. 5 Reusability of Pd_{NPs}@B-SNTs under optimized conditions.

CO_2Ee, OH and H) toward the synthesis of the desired amides, moderate to good reactivity was observed. Aromatic amines with electron-withdrawing groups on the aromatic ring provided higher yield in the synthesis of amides (Table 5). In the case of aliphatic alcohols, inferior yields were observed when compared to aromatic alcohols, which might be due to the side reactions such as oxidation to the corresponding carboxylic acids or aldol condensation. In addition to aniline, other amines such as pyrrolidine, diphenylamine, and phenyl methanamine were evaluated, and the results are summarized in Table 5.

As explained in the literature,[73,74] in the case of a plausible mechanism for the oxidation of alcohols, it can be said that at first the active site of the Pd_{NPs} interacts with H_2O_2 to form the Pd_{NPs} peroxo complex (I). The complex then reacts with benzyl alcohol, which leads to the formation of intermediate (II), which eventually regenerates the active sites of benzyl alcohol by two steps of dehydration and forms benzaldehyde. The primary

Table 6 The recyclability of Pd_{NPs}@B-SNTs and reuse during the synthesis of various amides[a]

Cycle	Scale (mol)	Leaching (ppm)	Yield[b] (%)
1	1	0.1	95/92
2	0.8	0.15	95/92
3	0.78	0.25	90/88
4	0.74	0.38	88/85
5	0.7	0.4	88/88
6	0.65	0.48	85/85
7	0.62	0.53	83/83
8	0.58	0.58	83/83

[a] Benzyl alcohol (1 mmol), amine source (1.2 mmol), base (1.5 mmol), H_2O_2 (4 mmol) and Pd_{NPs}@B-SNTs (1.5 mol% of Pd); 15–20 h. [b] Isolated yields.

amide formation mechanism proceeds through the reaction of an aldehyde with hydroxylammonium chloride in the presence of palladium with the formation of an aldoxime–PD_{NPs} intermediate. Then, during the dehydration process, intermediate (I) forms. Finally, hydration of intermediate (I) leads to the formation of intermediate (II) and completes the catalytic cycle *via* dehydration processes.[75] For secondary amides, the reaction mechanism involves oxidation and/or rearrangement *via* hydroperoxide intermediates formed from hemiaminal intermediates and/or imine intermediates.[76] As shown in Scheme 2, the reaction mechanism involves the formation of a peroxide mediator in the oxidative process.

To further assess the performance of Pd_{NPs}@B-SNTs, the stability and reusability of Pd_{NPs}@B-SNTs toward the amidation reaction according to the model reaction were investigated. After the completion of the reaction, the catalyst and the product (Pd_{NPs}@B-SNTs + amide) were isolated from the reaction mixture using a biphasic system, and the catalyst was precipitated in the aqueous phase. After several washes, the catalyst was dried for 6 h at 70 °C and was reused for the next recycling run. We found that in addition to the high stability, the Pd_{NPs}@B-SNT catalyst can be reused for up to 8 consecutive cycles without noticeable loss of activity (Fig. 5a). The TEM image and the atomic absorption spectrometry (AAS) of Pd_{NPs}@B-SNTs after 8 successive uses also confirmed this fact and shows that the nanoparticles demonstrated reduced leaching (Fig. 5b).

A controlled leaching experiment was performed to attain an understanding of the heterogeneous nature of Pd_{NPs}@B-SNTs. The results of atomic absorption spectrometry (AAS) showed that after 8 runs, the leaching of Pd is below 1.0 ppm in each cycle. Thus, the AAS analysis confirmed that the Pd_{NPs}@B-SNT catalyst is heterogeneous in nature. The leaching of Pd_{NPs}@B-SNTs is quantified and presented in Table 6.

The results of our work in comparison with catalysts previously reported in the literature are summarized in Table 7. As can be seen, this catalyst exhibited good catalytic activity with excellent yields (up to 95%) in mild conditions compared to most of the reported works.

Table 7 Comparison of different methods used in the synthesis of various amides using different reagents and reaction conditions

Entry	Catalyst	Oxidant	Solvent	T (°C)	Time (h)	Yield (%)	Ref.
1	MnO_2	O_2	Toluene	100	24	57	11
2	GO/Pd_{NPs}	H_2O_2	H_2O	25	15–24	94	68
3	MnO_2/GO	O_2	H_2O	150	3–30	98	13
4	PS-BHA-Cu	TBHP	DMF–H_2O	80	5	99	8
5	AuPd/resin	H_2O	O_2	40	12	49–99	77
6	$CuSO_4 \cdot 5H_2O$	TBHP	Acetonitrile	80	24	46–93	7
7	$FeCl_3$	EDC	TEMPO	90	8–32	75–92	10
8	Pd_{NPs}@B-SNTs	H_2O	H_2O_2	25–80	15–20	95	This work

4. Conclusion

In summary, we developed a sustainable and green catalytic protocol using encapsulated palladium nanoparticles within B-SNT organosilica cavities to synthesize a wide variety of amides using two different methods. All of the results indicate the high potential of Pd_{NPs}@B-SNTs as an exceptional hybrid catalyst for the amidation reaction under mild conditions with excellent performance. In this work, H_2O_2 was used as a mild and inexpensive oxidant, in accordance with the green chemistry landscape, as a promising oxidant and only produced water as a by-product. Due to the desirable results in this work, the high performance of this protocol can be studied for other cases, which will be reported in subsequent works.

Conflicts of interest

The authors declare no competing financial interests.

References

1 V. R. Pattabiraman and J. W. Bode, *Nature*, 2011, **480**, 471–479.
2 J. R. Dunetz, J. Magano and G. A. Weisenburger, *Org. Process Res. Dev.*, 2016, **20**, 140–177.
3 G. Li and M. Szostak, *Nat. Commun.*, 2018, **9**, 1–8.
4 J. Gu, Z. Fang, C. Liu, Z. Yang, X. Li, P. Wei and K. Guo, *RSC Adv.*, 2015, **5**, 95014–95019.
5 X.-F. Wu, M. Sharif, J.-B. Feng, H. Neumann, A. Pews-Davtyan and P. Langer, *Green Chem.*, 2013, **15**, 1956–1961.
6 S. Gaspa, A. Porcheddu and L. De Luca, *Org. Biomol. Chem.*, 2013, **11**, 3803–3807.
7 J. Gu, Z. Fang, Y. Yang, Z. Yang, L. Wan, X. Li, P. Wei and K. Guo, *RSC Adv.*, 2016, **6**, 89413–89416.
8 R. A. Molla, K. Ghosh, K. Tuhina and S. Manirul Islam, *New J. Chem.*, 2015, **39**, 921–930.
9 G. Wang, Q. Y. Yu, S. Y. Chen and X. Q. Yu, *Org. Biomol. Chem.*, 2014, **12**, 414–417.
10 R. Das and D. Chakraborty, *Catal. Commun.*, 2012, **26**, 48–53.
11 T. Ishida, H. Watanabe, T. Takei, A. Hamasaki, M. Tokunaga and M. Haruta, *Appl. Catal., A*, 2012, **425–426**, 85–90.

12 F. Paquin, J. Rivnay, A. Salleo, N. Stingelin and C. Silva, *J. Mater. Chem. C*, 2015, **3**, 10715–10722.
13 R. Nie, J. Shi, S. Xia, L. Shen, P. Chen, Z. Hou and F. S. Xiao, *J. Mater. Chem.*, 2012, **22**, 18115–18118.
14 K. Yamaguchi, H. Kobayashi, T. Oishi and N. Mizuno, *Angew. Chem., Int. Ed.*, 2012, **51**, 544–547.
15 D. Q. Dong, S. H. Hao, H. Zhang and Z. L. Wang, *Chin. Chem. Lett.*, 2017, **28**, 1597–1599.
16 X. Guo, L. Tang, Y. Yang, Z. Zha and Z. Wang, *Green Chem.*, 2014, **16**, 2443–2447.
17 N. A. Owston, A. J. Parker and J. M. J. Williams, *Org. Lett.*, 2007, **9**, 73–75.
18 X. Bantreil, C. Fleith, J. Martinez and F. Lamaty, *ChemCatChem*, 2012, **4**, 1922–1925.
19 X. F. Wu, M. Sharif, A. Pews-Davtyan, P. Langer, K. Ayub and M. Beller, *Eur. J. Org. Chem.*, 2013, 2783–2787.
20 A. Wang, J. Li and T. Zhang, *Nat. Rev. Chem.*, 2018, **2**, 65–81.
21 L. B. Sun, X. Q. Liu and H. C. Zhou, *Chem. Soc. Rev.*, 2015, **44**, 5092–5147.
22 Y. Wang, H. Arandiyan, J. Scott, A. Bagheri, H. Dai and R. Amal, *J. Mater. Chem. A*, 2017, **5**, 8825–8846.
23 W. Wang, J. E. Lofgreen and G. A. Ozin, *Small*, 2010, **6**, 2634–2642.
24 Y. Wu, Y. Zhang, J. Zhou and D. Gu, *Emergent Mater.*, 2020, **3**, 247–266.
25 S. Omar and R. Abu-Reziq, *J. Phys. Chem. C*, 2014, **118**, 30045–30056.
26 J. Dai, H. Zou, R. Wang, Y. Wang, Z. Shi and S. Qiu, *Green Chem.*, 2017, **19**, 1336–1344.
27 S. Elavarasan, K. Kala, I. Muhammad, A. Bhaumik and M. Sasidharan, *Mol. Catal.*, 2019, **476**, 110521.
28 M. Chen, C. Liang, F. Zhang and H. Li, *ACS Sustainable Chem. Eng.*, 2014, **2**, 486–492.
29 H. Naeimi, V. Nejadshafiee and S. Masoum, *RSC Adv.*, 2015, **5**, 15006–15016.
30 L. Bourda, H. S. Jena, R. Van Deun, A. M. Kaczmarek and P. Van Der Voort, *J. Mater. Chem. A*, 2019, **7**, 14060–14069.
31 E. Doustkhah, S. Rostamnia, M. Imura, Y. Ide, S. Mohammadi, C. J. T. Hyland, J. You, N. Tsunoji, B. Zeynizadeh and Y. Yamauchi, *RSC Adv.*, 2017, **7**, 56306–56310.
32 A. Eftekhari, M. Dalili, Z. Karimi, S. Rouhani, A. Hasanzadeh, S. Rostamnia, S. Khaksar, A. O. Idris, H. Karimi-Maleh and M. L. Yola, *Food Chem.*, 2021, **358**, 129763.
33 E. Doustkhah, H. Mohtasham, M. Farajzadeh, S. Rostamnia, Y. Wang, H. Arandiyan and M. H. N. Assadi, *Microporous Mesoporous Mater.*, 2020, **293**, 109832.
34 E. Doustkhah, H. Mohtasham, M. Hasani, Y. Ide, S. Rostamnia, N. Tsunoji and M. H. N. Assadi, *Mol. Catal.*, 2020, **482**, 110676.
35 A. Ahadi, H. Alamgholiloo, S. Rostamnia, X. Liu, M. Shokouhimehr, D. A. Alonso and R. Luque, *ChemCatChem*, 2019, **11**, 4803–4809.
36 A. G. Moaser, A. Ahadi, S. Rouhani, B. B. Mamba, T. A. M. Msagati, S. Rostamnia, T. Kavetskyy, S. Dugheri, S. Khaksar, A. Hasanzadeh and M. Shokouhimehr, *J. Mol. Liq.*, 2020, **312**, 113388.
37 A. Hasanzadeh, B. Gholipour, S. Rostamnia, A. Eftekhari, A. Tanomand, S. Khaksar and R. Khalilov, *J. Colloid Interface Sci.*, 2021, **585**, 676–683.
38 X. Liu, X. Li, Z. Guan, J. Liu, J. Zhao, Y. Yang and Q. Yang, *Chem. Commun.*, 2011, **47**, 8073–8075.
39 S. Zhang, H. Wang, M. Li, J. Han, S. Inagaki and X. Liu, *Dalton Trans.*, 2017, **46**, 9369–9374.
40 M. Li, H. Wang, X. Li, S. Zhang, J. Han, A. F. Masters, T. Maschmeyer and X. Liu, *ChemCatChem*, 2018, **10**, 581–589.
41 S. Zhang, X. Liu, M. Li, Y. Wei, G. Zhang, J. Han, X. Zhu, Q. Ge and H. Wang, *Catal. Today*, 2019, **324**, 59–65.
42 S. Rostamnia, X. Liu and D. Zheng, *J. Colloid Interface Sci.*, 2014, **432**, 86–91.
43 E. Doustkhah, S. Rostamnia, H. G. Hossieni and R. Luque, *ChemistrySelect*, 2017, **2**, 329–334.
44 H. Alamgholiloo, S. Rostamnia and N. Noroozi Pesyan, *Appl. Organomet. Chem.*, 2020, **34**, e5452.
45 S. Rostamnia, E. Doustkhah and A. Nuri, *J. Fluorine Chem.*, 2013, **153**, 1–6.
46 S. Rostamnia and E. Doustkhah, *Tetrahedron Lett.*, 2014, **55**, 2508–2512.
47 S. Rostamnia and T. Rahmani, *Appl. Organomet. Chem.*, 2015, **29**, 471–474.
48 S. Rostamnia and E. Doustkhah, *J. Mol. Catal. A: Chem.*, 2016, **411**, 317–324.
49 S. Rostamnia, H. G. Hossieni and E. Doustkhah, *J. Organomet. Chem.*, 2015, **791**, 18–23.
50 S. Rostamnia and E. Doustkhah, *Synlett*, 2015, **26**, 1345–1347.
51 S. Rostamnia, K. Lamei and F. Pourhassan, *RSC Adv.*, 2014, **4**, 59626–59631.
52 S. Rostamnia, A. Hassankhani, H. G. Hossieni, B. Gholipour and H. Xin, *J. Mol. Catal. A: Chem.*, 2014, **395**, 463–469.
53 S. Rostamnia, B. Gholipour and H. G. Hosseini, *Process Saf. Environ. Prot.*, 2016, **100**, 74–79.
54 M. Farajzadeh, H. Alamgholiloo, F. Nasibipour, R. Banaei and S. Rostamnia, *Sci. Rep.*, 2020, **10**, 1–9.
55 S. Rostamnia, K. Lamei and F. Pourhassan, *RSC Adv.*, 2015, **5**, 1033.
56 N. Nouruzi, M. Dinari, N. Mokhtari, B. Gholipour, S. Rostamnia, S. Khaksar and R. Boluki, *Appl. Organomet. Chem.*, 2020, **34**, 1–10.
57 S. Rostamnia and A. Morsali, *RSC Adv.*, 2014, **4**, 10514–10518.
58 H. G. Hosseini, E. Doustkhah, M. V. Kirillova, S. Rostamnia, G. Mahmoudi and A. M. Kirillov, *Appl. Catal., A*, 2017, **548**, 96–102.
59 H. Golchin Hosseini and S. Rostamnia, *New J. Chem.*, 2018, **42**, 619–627.
60 A. Hassankhani, B. Gholipour and S. Rostamnia, *Polyhedron*, 2020, **175**, 114217.
61 H. Mohtasham, B. Gholipour, S. Rostamnia, A. Ghiasi-Moaser and M. Shokouhimehr, *Colloids Surf., A*, 2021, **614**, 126187.

62 S. Rostamnia and S. Kholdi, *Adv. Powder Technol.*, 2018, **29**, 1167–1174.
63 S. Rostamnia, B. Gholipour, X. Liu, Y. Wang and H. Arandiyan, *J. Colloid Interface Sci.*, 2018, **511**, 447–455.
64 S. Rostamnia and M. Jafari, *Appl. Organomet. Chem.*, 2017, **31**, 1–6.
65 S. Rostamnia, E. Doustkhah and B. Zeynizadeh, *Microporous Mesoporous Mater.*, 2016, **222**, 87–93.
66 S. Rostamnia, E. Doustkhah and B. Zeynizadeh, *J. Mol. Catal. A: Chem.*, 2016, **416**, 88–95.
67 S. Rostamnia, N. Nouruzi, H. Xin and R. Luque, *Catal. Sci. Technol.*, 2015, **5**, 199–205.
68 S. Rostamnia, E. Doustkhah, H. Golchin-Hosseini, B. Zeynizadeh, H. Xin and R. Luque, *Catal. Sci. Technol.*, 2016, **6**, 4124–4133.
69 A. Alizadeh, N. Zohreh and S. Rostamnia, *Tetrahedron*, 2007, **63**, 8083–8087.
70 K. Zhu, Y. Du, J. Liu, X. Fan, Z. Duan, G. Song, A. Meng, Z. Li and Q. Li, *J. Nanosci. Nanotechnol.*, 2017, **17**, 2515–2519.
71 P. Van Der Voort, D. Esquivel, E. De Canck, F. Goethals, I. Van Driessche and S. S. Francisco Romero, *Chem. Soc. Rev.*, 2013, **42**, 3913–3955.
72 E. De Canck, *Versatile Hybrid Nanomaterials: Periodic Mesoporous Organosilicas as Adsorbent and Catalyst*, 2013.
73 Y. Yu, B. Lu, X. Wang, J. Zhao, X. Wang and Q. Cai, *Chem. Eng. J.*, 2010, **162**, 738–742.
74 X. Xia, X. Gao, J. Xu, C. Hu and X. Peng, *J. Saudi Chem. Soc.*, 2017, **21**, 334–340.
75 M. A. Ali and T. Punniyamurthy, *Adv. Synth. Catal.*, 2010, **352**, 288–292.
76 Y. Suto, N. Yamagiwa and Y. Torisawa, *Tetrahedron Lett.*, 2008, **49**, 5732–5735.
77 L. Zhang, W. Wang, A. Wang, Y. Cui, X. Yang, Y. Huang, X. Liu, W. Liu, J. Y. Son, H. Oji and T. Zhang, *Green Chem.*, 2013, **15**, 2680–2684.